Signatures of bifurcation on quantum correlations: Case of the quantum kicked top

Udaysinh T. Bhosale* and M. S. Santhanam†
Indian Institute of Science Education and Research, Dr. Homi Bhabha Road, Pune 411 008, India
(Received 21 October 2016; published 27 January 2017)

Quantum correlations reflect the quantumness of a system and are useful resources for quantum information and computational processes. Measures of quantum correlations do not have a classical analog and yet are influenced by classical dynamics. In this work, by modeling the quantum kicked top as a multiqubit system, the effect of classical bifurcations on measures of quantum correlations such as the quantum discord, geometric discord, and Meyer and Wallach Q measure is studied. The quantum correlation measures change rapidly in the vicinity of a classical bifurcation point. If the classical system is largely chaotic, time averages of the correlation measures are in good agreement with the values obtained by considering the appropriate random matrix ensembles. The quantum correlations scale with the total spin of the system, representing its semiclassical limit. In the vicinity of trivial fixed points of the kicked top, the scaling function decays as a power law. In the chaotic limit, for large total spin, quantum correlations saturate to a constant, which we obtain analytically, based on random matrix theory, for the Q measure. We also suggest that it can have experimental consequences.

DOI: 10.1103/PhysRevE.95.012216

I. INTRODUCTION

It is well established by more than half a century of quantum chaos research that many of the properties of quantum systems can be understood in terms of classical objects such as periodic orbits and their stability [1]. For classically integrable systems, the Einstein-Brillouin-Keller quantization method relates the quantum spectra and the classical action [2], while for chaotic systems Gutzwiller's trace formula represents such an approach connecting the quantum spectra and the classical periodic orbits [3]. The advent of quantum information and computation has opened up newer scenarios in which novel quantum correlations did not have corresponding classical analogues. Quantum entanglement is one such phenomenon without a classical analog. The von Neumann entropy, a measure of quantum entanglement for a bipartite pure state, captures correlations with purely quantum origins that are stronger than classical correlations. A host of such measures are now widely used in the quantum information theory to quantify stronger than classical correlations.

Quantum correlations do not have exact classical analogs, yet they are surprisingly affected by the classical dynamics. For instance, in the context of chaotic systems, it is known that upon variation of a parameter, as chaos increases in the system the entanglement also increases and saturates to a value predicted based on random matrix theory (RMT) [4]. Recently, this was experimentally demonstrated for an isolated quantum system consisting of three superconducting qubits as a realization of the quantum kicked top [5]. It was shown that larger values of entanglement correspond to regimes of chaotic dynamics [6]. Theoretically, not just the chaotic dynamics but indeed the structure and details of classical phase space, such as the presence of elliptic islands in a sea of chaos, are known to affect the entanglement [7].

Quantum entanglement is an important resource for quantum information processing and computational tasks. However, it does not capture all the correlations in a quantum system. It is possible for unentangled states to display nonclassical behavior, implying that there might be residual quantum correlations beyond what is measured by entanglement. In addition, it is now known that entanglement is not the only ingredient responsible for speedup in quantum computing [8–10]. For the mixed-state quantum computing model, discrete quantum computation with one qubit (DQC1), experiments have shown that some tasks can be speeded up over their classical counterparts even using nonentangled, i.e., separable states but having nonzero quantum correlations [11–13]. Hence, quantification of *all* possible quantum correlations is important. For this purpose, measures like quantum discord [14,15], geometric discord [16,17], Leggett-Garg inequality [18], and a host of others are widely used.

Quantum discord is independent of entanglement and no simple ordering relations between them is known [19,20]. Entanglement may be larger than quantum discord even though for separable states entanglement always vanishes but quantum discord may be nonzero and, thus, is less than quantum discord [20–22]. This shows that discord and in general all quantum correlation measures are more fundamental than entanglement [23]. It is shown that two-qubit quantum discord in a dissipative dynamics under Markovian environments vanishes only in the asymptotic limit where entanglement suddenly disappears [24]. Thus, the quantum algorithms that make use of quantum correlations, represented in discord, might be more robust than those based on entanglement [24]. This shows that studying quantum correlation, in general, in a given system is important from the point of view of decoherence, which is inevitably present in almost all experimental setups.

In the last decade, many experimental and theoretical studies of discord were performed [25]. A recent experiment realizes quantum advantage with zero entanglement but with nonzero quantum discord using a single photon's polarization and its path as two qubits [26]. Other experiments have estimated the discord in an antiferromagnetic Heisenberg compound [27] and in Bell-diagonal states [28]. In the context of chaotic systems, e.g., the quantum kicked top, the dynamics of discord reveals the classical phase-space structure [29]. In

*udaybhosale0786@gmail.com
†santh@iiserpune.ac.in

this paper, we show that a period-doubling bifurcation [30] in the kicked top leaves its signature in the dynamics of quantum correlation measures such as discord and geometric discord, including the multipartite entanglement measure, the Meyer and Wallach Q measure [31].

The structure of the paper is as follows: In Sec. II the measures of quantum correlations used are introduced. In Sec. III the kicked-top model is introduced. In Sec. IV results on the effects of the bifurcation on the time averages of these measures of quantum correlations are given. In Sec. V these results are compared with a suitable random matrix model. In Sec. VI scaling of these time-averaged measures is studied as a function of the total spin.

II. MEASURE OF QUANTUM CORRELATIONS

A. Quantum discord

Quantum discord is a measure of all possible quantum correlations including and beyond entanglement in a quantum state. In this approach one removes the classical correlations from the total correlations of the system. For a bipartite quantum system, its two parts, labeled A and B and represented by its density matrix ρ_{AB}, if the von Neumann entropy is $\mathcal{H}(\rho_{AB}) = -\mathrm{Tr}(\rho_{AB}\log\rho_{AB})$, then the total correlations is quantified by the quantum mutual information as

$$\mathcal{I}(B:A) = \mathcal{H}(B) + \mathcal{H}(A) - \mathcal{H}(B,A). \tag{1}$$

In classical information theory, the mutual information based on Baye's rule is given by

$$I(B:A) = H(B) - H(B|A), \tag{2}$$

where $H(B)$ is the Shannon entropy of B. The conditional entropy $H(B|A)$ is the average of the Shannon entropies of system B conditioned on the values of A. It can be interpreted as the ignorance of B given the information about A.

Quantum measurements on subsystem A are represented by a positive operator-valued measure (POVM) set $\{\Pi_i\}$, such that the conditioned state of B given outcome i is

$$\rho_{B|i} = \mathrm{Tr}_A(\Pi_i\rho_{AB})/p_i \quad \text{and} \quad p_i = \mathrm{Tr}_{A,B}(\Pi_i\rho_{AB}), \tag{3}$$

and its entropy is $\tilde{\mathcal{H}}_{\{\Pi_i\}}(B|A) = \sum_i p_i\mathcal{H}(\rho_{B|i})$. In this case, the quantum mutual information is $\mathcal{J}_{\{\Pi_i\}}(B:A) = \mathcal{H}(B) - \tilde{\mathcal{H}}_{\{\Pi_i\}}(B|A)$. Maximizing this over the measurement sets $\{\Pi_i\}$ we get

$$\begin{aligned}\mathcal{J}(B:A) &= \max_{\{\Pi_i\}}\left(\mathcal{H}(B) - \tilde{\mathcal{H}}_{\{\Pi_i\}}(B|A)\right)\\ &= \mathcal{H}(B) - \tilde{\mathcal{H}}(B|A)E,\end{aligned} \tag{4}$$

where $\tilde{\mathcal{H}}(B|A) = \min_{\{\Pi_i\}}\tilde{\mathcal{H}}_{\{\Pi_i\}}(B|A)$. The minimum value is achieved using rank 1 POVMs since the conditional entropy is concave over the set of convex POVMs [32]. By taking $\{\Pi_i\}$ as rank 1 POVMs, quantum discord is defined as $\mathcal{D}(B:A) = \mathcal{I}(B:A) - \mathcal{J}(B:A)$, such that

$$\mathcal{D}(B:A) = \mathcal{H}(A) - \mathcal{H}(B,A) + \min_{\{\Pi_i\}}\tilde{\mathcal{H}}_{\{\Pi_i\}}(B|A). \tag{5}$$

Quantum discord is nonnegative for all quantum states [14,32,33] and is subadditive [34].

B. Geometric discord

The calculation of discord involves the maximization of $J(A:B)$ by doing measurements on subsystem B, which is a hard problem. A more easily computable form is geometric discord based on a geometric method [16,17]. There are no measurements involved in calculating this measure. For the special case of two qubits a closed-form expression is given [16]. The dynamics of geometric discord is studied under a common dissipating environment [35]. For every quantum state there is a set of postmeasurement classical states, and the geometric discord is defined as the distance between the quantum state and the nearest classical state,

$$D^G(B|A) = \min_{\chi\in\Omega_0}\|\rho - \chi\|^2, \tag{6}$$

where Ω_0 represents the set of classical states, and $\|X - Y\|^2 = \mathrm{Tr}[(X-Y)^2]$ is the Hilbert-Schmidt quadratic norm. Obviously, $D^G(B|A)$ is invariant under local unitary transformations. The explicit and tight lower bound on the geometric discord for an arbitrary state of a bipartite quantum system $A_{m\times m}\otimes B_{n\times n}$ is available [17,36,37]. Recently discovered ways to calculate lower bounds on discord for such general states do not require tomography and, hence, are experimentally realizable [36,37].

Following the formalism of Dakic *et al.* [16] the analytical expression for the geometric discord for two-qubit states is obtained. The two-qubit density matrix in the Bloch representation is

$$\rho = \frac{1}{4}\left(\mathbb{1}\otimes\mathbb{1} + \sum_{i=1}^{3}x_i\sigma_i\otimes\mathbb{1} + \sum_{i=1}^{3}y_i\mathbb{1}\otimes\sigma_i + \sum_{i,j=1}^{3}T_{ij}\sigma_i\otimes\sigma_j\right), \tag{7}$$

where x_i and y_i represent the Bloch vectors for the two qubits, and $T_{ij} = \mathrm{Tr}[\rho(\sigma_i\otimes\sigma_j)]$ are the components of the correlation matrix. The geometric discord for such a state is

$$D^G(B|A) = \tfrac{1}{4}(\|x\|^2 + \|T\|^2 - \eta_{\max}), \tag{8}$$

where $\|T\|^2 = \mathrm{Tr}[T^TT]$, and $\eta_{\max}$ is the largest eigenvalue of $\vec{x}\vec{x}^T + TT^T$, whose explicit form is given in [38].

C. Meyer and Wallach Q measure

In this work, the effects of bifurcation on multipartite entanglement are also studied using the Meyer and Wallach Q measure [31]. This was used to study the multipartite entanglement in spin Hamiltonians [39–41] and systems of spin bosons [42]. The geometric multipartite entanglement measure Q is shown to be simply related to one-qubit purities [43]. Calculating and interpreting it are straightforward. If ρ_i is the reduced density matrix of the ith spin obtained by tracing out the rest of the spins in an N-qubit pure state, then

$$Q(\psi) = 2\left(1 - \frac{1}{N}\sum_{i=1}^{N}\mathrm{Tr}\left(\rho_i^2\right)\right). \tag{9}$$

This relation between Q and the single-spin reduced density matrix purities has led to a generalization of this measure to

multiqudit states and for various other bipartite splits of the chain [44].

III. KICKED TOP

The quantum kicked top is characterized by an angular momentum vector $\mathbf{J} = (J_x, J_y, J_z)$, whose components obey the standard angular momentum algebra. Here, Planck's constant is set to unity. The dynamics of the top is governed by the Hamiltonian [45]

$$H(t) = pJ_y + \frac{k}{2j}J_z^2 \sum_{n=-\infty}^{+\infty} \delta(t-n). \tag{10}$$

The first term represents the free precession of the top around the y axis at angular frequency p, and the second term is periodic δ kicks applied to the top. Each kick results in a torsion about the z axis by an angle $(k/2j)J_z$. The classical limit of Eq. (10) is integrable for $k = 0$ and becomes increasingly chaotic for $k > 0$. The period 1 Floquet operator corresponding to the Hamiltonian in Eq. (10) is given by

$$U = \exp\left(-i\frac{k}{2j}J_z^2\right)\exp(-ipJ_y). \tag{11}$$

The dimension of the Hilbert space is $2j+1$ so that the dynamics can be explored without truncating the Hilbert space. A kicked top was realized in experiments [46] and the range of parameters used in this work makes it experimentally feasible.

The quantum kicked top for a given angular momentum j can be regarded as a quantum simulation of a collection of $N = 2j$ qubits (spin-half particles) whose evolution is restricted to the symmetric subspace under the exchange of particles. The state vector is restricted to a symmetric subspace spanned by the basis states $\{|j,m\rangle; (m = -j, -j+1, \ldots, j)\}$ where $j = N/2$. It is thus a multiqubit system whose collective behavior is governed by the Hamiltonian in Eq. (10) and quantum correlations between any two qubits can be studied. The kicked top has served as a useful model to study entanglement [6,47–51] and its relation to classical dynamics [52].

The classical phase space shown in Fig. 1 is a function of coordinates θ and ϕ. In order to explore quantum dynamics in the kicked top, we construct spin-coherent states [53–56] pointing along the direction of θ_0 and ϕ_0 and evolve it under the action of the Floquet operator. The quantum correlations reported in this paper represent time averages obtained from the time-evolved spin-coherent state.

The classical map for the kicked top is [45,53]

$$X' = (X\cos p + z\sin p)\cos(k(z\cos p - X\sin p)) - Y\sin(k(z\cos p - X\sin p)), \tag{12a}$$

$$Y' = (X\cos p + Z\sin p)\sin(k(Z\cos p - X\sin p)) + Y\cos(k(Z\cos p - X\sin p)), \tag{12b}$$

$$Z' = -X\sin p + Z\cos pE. \tag{12c}$$

Since the dynamical variables (X,Y,Z) are restricted to the unit sphere, i.e., $X^2 + Y^2 + Z^2 = 1$, they can be parameterized in terms of the polar angle θ and the azimuthal angle ϕ as $X = \sin\theta\cos\phi$, $Y = \sin\theta\sin\phi$, and $Z = \cos\theta$. We evolve the map in Eq. (12) and determine the values of (θ,ϕ) using the inverse relations (not shown here). For $p = \pi/2$ additional symmetry properties lead to a simpler classical map, a case studied in detail in Refs. [29,51]. In this paper two cases, namely, $p = \pi/2$ and $p = 1.7$, are studied, which are different from the RMT point of view as explained in Sec. V.

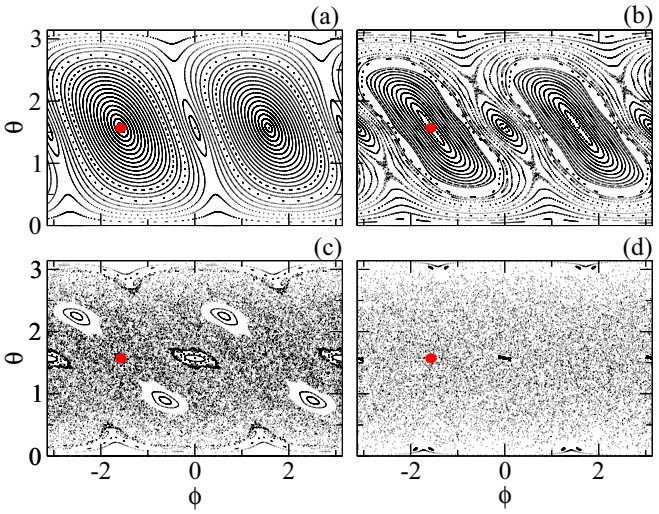

FIG. 1. Phase-space pictures of the classical kicked top for $p = \pi/2$ and (a) $k = 1$, (b) $k = 2$, (c) $k = 3$, and (d) $k = 6$. Filled red circles indicatethe initial position of the spin-coherent state.

IV. EFFECT OF BIFURCATION

First, we consider the case of $p = \pi/2$. If the kick strength is $k = 1$, then the phase space is largely dominated by invariant tori as shown in Fig. 1(a). In particular, the trivial fixed points of the map at $(\theta,\phi) = (\pi/2, \pm\pi/2)$ visible in Figs. 1(a) and 1(b) become unstable at $k = 2$. As k increases further, the new fixed points born at $k = 2$ move away [see Fig. 1(c)]. For $k = 6$, the phase space is largely chaotic, with no islands visible in Fig. 1(d). In the kicked top, the period-doubling bifurcation is the route for the regular-to-chaotic transition.

Second, here we study the case of $p = 1.7$. As shown in Figs. 2(a)–2(d), the phase space displays features similar to those in the case of $p = \pi/2$ except that the trivial fixed point $(\theta,\phi) = (\pi/2, -\pi/2)$ now loses stability at the numerically determined $k = 1.76$, while $(\theta,\phi) = (\pi/2,\pi/2)$ does so at $k = 2.2$. The black circle, marking the point $(\theta_0,\phi_0) = (\pi/2,-\pi/2)$ in Figs. 1 and 2, is the initial position of the spin-coherent-state wave packet.

To study the effect of bifurcation on the quantum correlation and multipartite entanglement measures, a multiqubit representation of the system is used. For a particular value of j the system can be decomposed into $N = 2j$ qubits. The reduced density matrix of two qubits is calculated by tracing out all other $N-2$ qubits [57,58] after every application of the Floquet map. We use the reduced density matrix to compute the various measures of correlation. As all the qubits are identical, the correlations measures do not depend on the actual choice of two qubits. Similarly, while calculating Q measure one needs to compute the reduced density matrix of only one qubit.

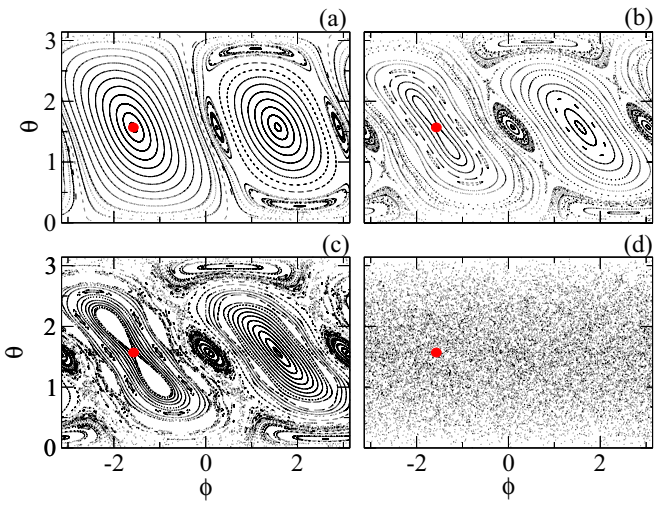

FIG. 2. Phase space of the classical kicked top for $p = 1.7$ and (a) $k = 1$, (b) $k = 1.9$, (c) $k = 2.1$, and (d) $k = 6$. Filled red circles indicate the initial position of the spin-coherent state.

The spin-coherent state at time $t = 0$, denoted $|\psi(0)\rangle$, is placed at the fixed point $(\theta,\phi) = (\pi/2,-\pi/2)$ (filled red circle in Figs. 1 and 2) undergoing a period-doubling bifurcation. The state $|\psi(0)\rangle$ is evolved by the Floquet operator $\hat{U}$ as $|\psi(n)\rangle = U^n|\psi(0)\rangle$. We apply the numerical iteration scheme given in Refs. [49,59] for time-evolving the initial state. At every time step, the discord D, geometric discord D^G, and Meyer and Wallach Q measure are calculated for a given value of k. The results shown in Figs. 3 and 4 represent time-averaged values of D, D^G, and Q for every k.

For both cases, $p = \pi/2$ (Fig. 3) and $p = 1.7$ (Fig. 4), the results are shown for two values of j, namely, $j = 50$ and $j = 120$. For comparison, the case of $j = 10$ qubits is also shown in Fig. 3. Broadly, in all cases, the quantum correlation measures D, D^G, and Q respond to the classical bifurcation in a similar manner: by displaying a jump in the mean value

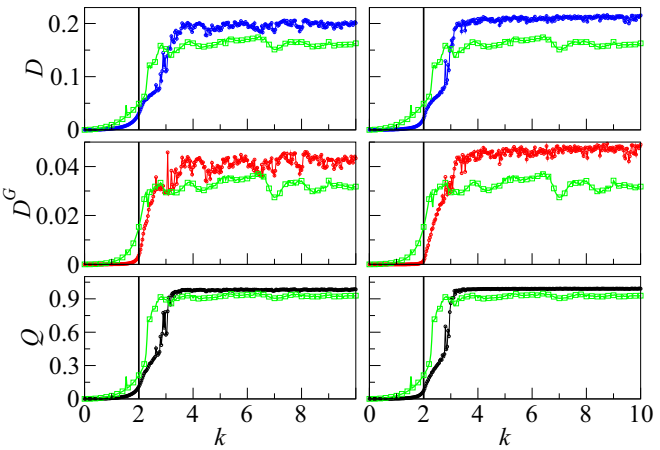

FIG. 3. Average discord, geometric discord, and Q measure as a function of k for $p = \pi/2$. Left column: $j = 50$. Right column: $j = 120$. For comparison purposes, the $j = 10$ case is represented in every graph as square green symbols. The vertical line marks the position of bifurcation at $k = 2$.

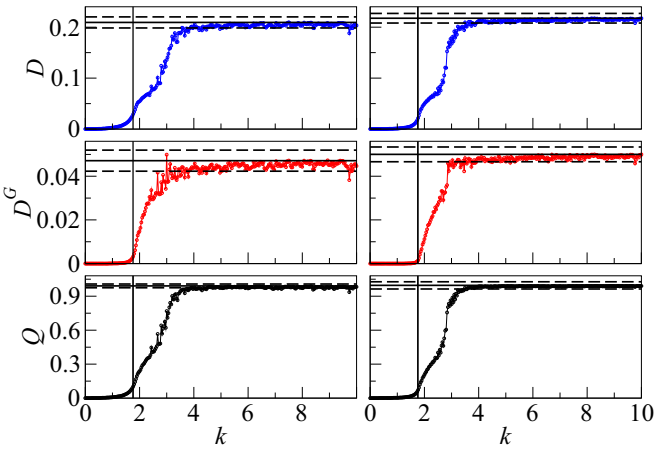

FIG. 4. Average discord, geometric discord, and Q measure as a function of k for $p = 1.7$. Left column: $j = 50$. Right column: $j = 120$. The solid horizontal line represents the long-time average of an initial state from the bifurcation point evolved using the operator U_{CUE}. The dashed line represents the standard deviation from the average value. The vertical line shows the position of bifurcation at approximately $k = 1.76$.

from about 0 to a nonzero value. This can be understood as follows. When the elliptic islands are large, as is the case when $0 < k < 2$ for $p = \pi/2$ and $0 < k < 1.76$ for $p = 1.7$, the evolution of the spin-coherent state placed initially at $(\theta,\phi) = (\pi/2,-\pi/2)$ is largely confined to the same elliptic islands. As the bifurcation point is approached, the local instability in the vicinity of the fixed point evolves part of the coherent state into the chaotic layers of phase space. This leads to an increase in the values of correlation measures. Note that increasing chaos leads to an increase in entanglement too. When j is increased, the width of coherent state $\sigma \propto 1/\sqrt{j}$ becomes narrower and closely mimics the classical evolution [53]. Thus, as j increases, we expect the quantum correlations to sharply respond to classical bifurcation at $k = 2$. Indeed, as shown in Fig. 3, the quantum correlations change sharply at $k = 2$ for $j = 120$ in comparison with the case for $j = 10$. To understand the details in Fig. 3 consider two values of j, e.g., $j = j_1$ and $j = j_2$, such that $j_2 > j_1$. The slow decay of σ as $j \to \infty$ implies that the response of quantum correlations to classical bifurcation becomes perceptible only when $|j_2 - j_1| \gg 1$. Thus, relative changes are easily seen when quantum correlations for $j = 120$ are compared with the $j = 10$ case rather than with that of $j = 50$. The approach to semiclassics, $\hbar \to 0$ limit, discussed in Sec. VI provides quantitative support of this picture.

V. CORRELATION MEASURES AND RANDOM MATRIX THEORY

Next, we show that the saturated values of D, D^G, and Q after bifurcation has taken place at $k = k_b$ can be obtained from random matrix considerations. The kicked top is time reversal invariant, and as a consequence its Floquet operator in the globally chaotic case has the statistical properties of a random matrix chosen from the circular orthogonal ensemble (COE) [60]. For the kicked top, the statistical properties of

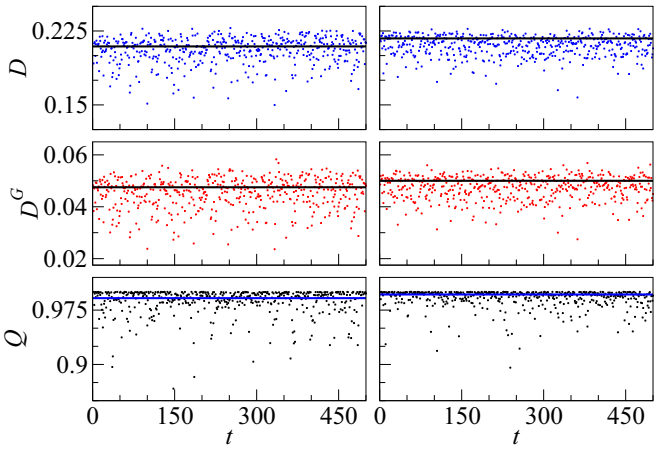

FIG. 5. Time variation of the correlation measures using the kicked-top Floquet operator for $j = 50$ (left) and for $j = 120$ (right) for the globally chaotic case ($k = 10$ and $p = 1.7$). The horizontal line corresponds to the time average of the correlation measures using a COE matrix of the respective case.

eigenvectors of its Floquet operator are in good agreement with the COE of random matrix theory [60]. Apart from time-reversal symmetry, the kicked top additionally has a parity symmetry, $\widehat{R}_y = \exp(-i\pi j_y)$, that commutes with the Floquet operator for all values of p. As $\widehat{R}_y^2 = I$, the eigenvalues of $\widehat{R}_y$ are $+1$ and -1. Thus, in the basis of the parity operator, the Floquet operator has a block-diagonal structure consisting of two blocks associated with the positive-parity ($+1$) or negative-parity (-1) eigenvalues. Thus, due to the parity symmetry, the kicked top is statistically equivalent to a block-diagonal random matrix (block diagonal in the basis in which the parity operator is diagonal) whose blocks (corresponding to the eigenvalues ± 1) are sampled from the COE [4]. If $p = \pi/2$, the kicked top possesses additional symmetries [60], a case which is not considered in this section. In this section, the case where $p = 1.7$ is studied in detail.

First, a block-diagonal COE, as the appropriate ensemble of random matrices for modeling the kicked-top Hamiltonian, is used. Since the basis here is that of eigenvectors of the parity operator $\widehat{R}_y$, this matrix is then written in the $|j,m\rangle$ basis. Finally, this matrix is used to evolve the coherent state and compared with the evolution done using the Floquet operator in the globally chaotic case ($k = 10$). The results are presented in Fig. 5 and summarized in Table I.

TABLE I. Mean value of correlation measures averaged over 1000 time steps of evolution of a coherent state with the Floquet matrix (with $k = 10$) and the COE matrix. COE values are represented in Fig. 4 as horizontal lines.

	$j = 50$		$j = 120$	
Measure	Floquet	COE	Floquet	COE
Discord	0.205	0.209	0.217	0.217
Geometric discord	0.045	0.047	0.049	0.050
Q measure	0.986	0.991	0.994	0.996

Figure 5 shows the evolution of the two-qubit discord, geometric discord, and Meyer-Wallach Q measure for $j = 50$ and $j = 120$ when acted on by the kicked-top Floquet operator with $k = 10$. At this kick strength the classical phase space of the kicked top is largely chaotic, with no visible regular regions. As Fig. 5 and Table I reveal, the dynamics of various correlation measures under the action of the COE matrix is similar to that of the kicked-top Floquet operator in its chaotic regime with $k = 10$. While this is not entirely unexpected, the values of the three measures listed in Table I closely agree with those obtained after bifurcation takes place at $k = k_b$, but at values of kick strengths much less than 10 considered in Fig. 5. Time averages listed in Table I are plotted in Fig. 4 along with the standard deviation of the individual measures. It can be seen that agreement between these values and that of the Floquet operator begins to emerge at around $k = 4$, which is much less than $k = 10$. The position of the coherent state in this case is $(\theta,\phi) = (\pi/2,-\pi/2)$. It should be noted that in the globally chaotic case these results are independent of the initial position of the coherent state.

It can be seen in Table I and Fig. 4 that the time averages of quantum correlations for the kicked top are systematically, although slightly, lower than those predicted by the circular orthogonal ensemble of random matrix theory. The agreement improves as $j \to \infty$. Hence, these deviations can be attributed to a finite-j effect. Similar systematic deviations from RMT were observed in a study of the log-negativity in the kicked rotor system [61]. In that case too, the deviations decreased as the corresponding Hilbert-space dimensions were increased.

VI. SCALING WITH THE PLANCK VOLUME

The kicked top is a finite-dimensional quantum system and the volume of its Planck cell is $V = 4\pi/(2j+1)$. For large j, $V \propto 1/j$. It is natural to ask how the measures of quantum correlation scale with this volume when the kick strength corresponds to $k = k_b$, where k_b is a bifurcation point. In Fig. 6, we show the variation in the time average of D, D^G, and Q as a function of j for $k = k_b$. Here, $k_b = 2$ and $p = \pi/2$. The coherent state is placed at the corresponding trivial fixed point $(\theta,\phi) = (\pi/2,-\pi/2)$ and the time average is taken over 500 steps. For $j \gg 1$, the correlation measures scale with j approximately in a power law of the form $j^{-\mu}$, where μ is the scaling exponent. The power-law fits through linear regression for the numerically computed correlations measures shown in Fig. 6 are consistent with

$$D \propto j^{-\mu_1}, \quad D^G \propto j^{-\mu_2}, \quad \text{and} \quad Q \propto j^{-\mu_3}, \tag{13}$$

where $\mu_1 = 0.382 \pm 0.003$, $\mu_2 = 0.944$, and $\mu_3 = 0.451$. The uncertainty values are estimated by numerical linear regression The uncertainties in the estimates for μ_2 and μ_3 are of the order of 10^{-8} and hence negligible. Identical power-law scaling is obtained for the other trivial fixed point at $(\theta,\phi) = (\pi/2,\pi/2)$, with exponents μ_i approximately the same as given in Eq. (13). The quantum correlations tend to 0 as $V \to 0$ ($j \to \infty$), indicating that for any finite j, quantum correlations, however small, would continue to exist. As the wave packet becomes more "classical" and the underlying dynamics is regular, we expect the quantum correlations to decrease with j. This is another indication that the regular regions in the vicinity of

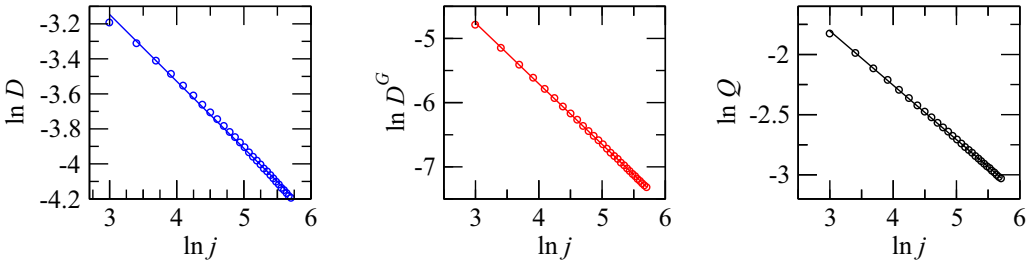

FIG. 6. Variation of time-averaged quantum correlations (circles) as a function of j. Lines are the power-law fits given in Eq. (13).

the fixed point undergoing bifurcations affect the quantum correlations deep in the semiclassical regime.

The appearance of power-law scaling can be understood for the case $k = 2$ when the regular region is large and the chaotic layer is a tiny fraction of the entire phase space. The presence of the chaotic layer has a strong influence on quantum correlations. Note that for $j \gg 1$, the width of the spin-coherent state $\sigma = j^{-1/2}$ becomes small and its evolution is mostly confined to the large elliptic islands in Figs. 1(a) and 1(b). As a result, it can be argued that the strength of the overlap of coherent state with the chaotic layer is indicative of quantum correlations. Since $\sigma = j^{-1/2}$, for $j \gg 1$, this overlap is small. The slow power-law decay of σ might possibly be the reason for the similar decay of quantum correlations as well, as shown in Eq. (13). Since quantum correlations are affected by the local phase-space features, a complete quantitative explanation of power-law scaling might require a detailed semiclassical analysis.

Next, we consider the case of a coherent state placed initially at a bifurcation point leading to a period 2 cycle. The origin of this bifurcation point is as follows. The trivial fixed points at $(\theta,\phi) = (\pi/2,\pm\pi/2)$ are easily visible in Figs. 1(a), 1(b), 2(a), and 2(b). If $p = \pi/2$, these fixed points bifurcate at $k = 2$ through a period-doubling bifurcation and become unstable. In the process, the point $(\theta,\phi) = (\pi/2,\pi/2)$ gives rise to two new period 1 stable fixed points, while the point $(\theta,\phi) = (\pi/2,-\pi/2)$ gives rise to a period 2 cycle. For $k > 2$ their positions move in the phase space as a function of k and they are stable for $k \leqslant \sqrt{2}\pi$. For $k > \sqrt{2}\pi$, the two fixed points bifurcate into two new period 2 cycles, while the period 2 cycle gives rise to a new period 4 cycle. Their positions for $k = \sqrt{2}\pi$ are shown in Fig. 7. Our interest lies in the fixed point located at $(\theta,\phi) = (\pi/4,0)$.

Figure 8 shows the variation of the time average of the quantum correlation measures as a function of j for the initial coherent state placed at this fixed point. It can be seen that after initial fluctuations the correlations start to decrease for larger values of j. It should be noted that the area of elliptic islands is continually shrinking as $k \to \infty$, consistent with the predominance of chaotic regions in the phase space. The width of the spin-coherent state $|\psi(0)\rangle$ is equal to $1/\sqrt{j}$. For small values of j, the width of $|\psi(0)\rangle$ is much larger than that of the regular elliptic island as shown in Fig. 7. Hence, there is a pronounced overlap of state $|\psi(0)\rangle$ with the chaotic sea. Hence we expect that for small j the quantum correlations will be reasonably close to their random matrix averages. This is indeed shown in Fig. 8 for $1 \leqslant j \leqslant 50$ as the width of $|\psi(0)\rangle$ is at least twice the size of the elliptic island. For $j \gg 1$, the width of $|\psi(0)\rangle$ has become much smaller than that of the elliptic island. Thus, under these conditions we expect smooth decay with increasing j, similar to what is shown in Figs. 6(a)–6(c). Figure 8 does show smooth decay for $j \gtrsim 150$. Thus, the quantum correlations, on average, decay as a function of j and the area of the regular region surrounding the fixed point undergoing bifurcation strongly affects the quantum correlations.

Now, we consider the kick strength $k = 10$ and place the spin-coherent state $|\psi(0)\rangle$ at an arbitrary position in the chaotic sea, namely, $(\theta,\phi) = (1.6707,1.3707)$. Here, the phase space is largely chaotic, devoid of any regular regions. In contrast to the results in Figs. 6 and 8, the time-averaged correlation measures shown in Fig. 9 increase with j. Based on the results in Figs. 4 and 5 we can expect that at every value of j the time-averaged D, D_G, and Q agree with those found using the appropriate COE ensemble.

For a coherent state the quantum correlation measures are 0. However, after time evolution, the correlation values will depend on the corresponding measures for Floquet eigenstates. Thus, it is important to study the typical values of these measures for these eigenstates. This can be analytically obtained for the average Q measure. An exact analytical formula for the average Q measure is derived (see the Appendix for the detailed derivation) for a typical COE ensemble modeling the Floquet operator in the globally chaotic case. It is given by

$$\langle Q\rangle_E = 1 - \frac{16j(j+1)}{3(2j+3)(2j+1)^2}. \tag{14}$$

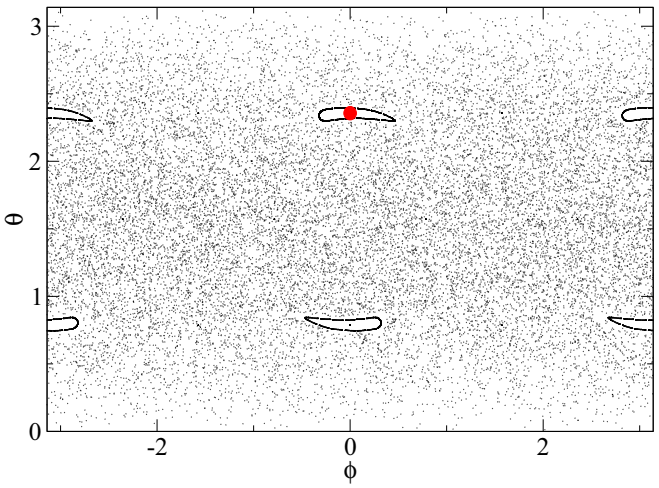

FIG. 7. Phase-space picture of the classical kicked top for $k = \sqrt{2}\pi$. Filled red circles indicate the initial position of the spin-coherent state.

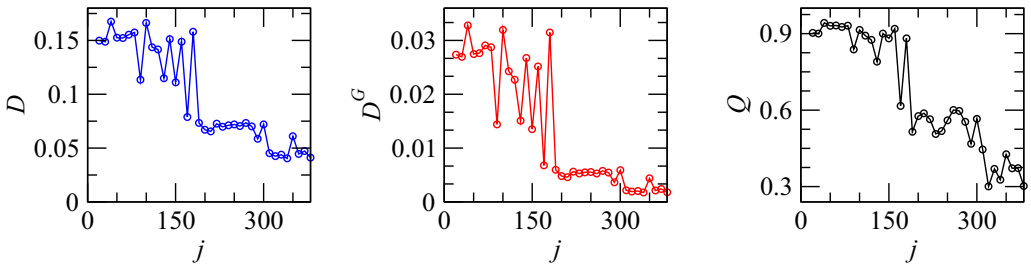

FIG. 8. Variation of time-averaged quantum correlations (circles connected by lines) as a function of j for $k = \sqrt{2}\pi$ and the initial position of the spin-coherent state as shown in Fig. 7.

For large j, $\langle Q\rangle_E \approx 1 - 2/(3j)$, implying that the measure tends to 1 for large j. The numerically computed correlations for the eigenvectors of the COE ensemble and for the eigenvectors of the Floquet operator under conditions of globally classical chaos are compared with the analytical result in Eq. (14) and Fig. 10.

For generating sufficient statistics for the eigenvectors of the Floquet operator, we use a range of k values such that the corresponding classical section does not have any significant regular islands and is highly chaotic. The analytical result in Eq. (14) agrees with that for the eigenvectors of the COE. In order to derive similar expressions for the average discord and geometric discord for the eigenvectors of the COE, the analytical expression for the distribution of the matrix elements of the two-qubit density matrix for this class of states is required. Such an expression is not known yet, to the best of our knowledge. Thus, the derivation of the average discord and geometric discord as a function of j remains an open question.

It is instructive to compare these results with those for other well-studied ensembles such as the Gaussian ensembles. In this case, the states are distributed uniformly, also known as the Haar measure, on the unit sphere. Consider a tripartite random pure state. The entanglement between any of its two subsystems shows a transition from an entangled to a separable state as the size of the third subsystem is increased [61,62]. Another example is that of definite particle states. This shows algebraic to exponential decay of entanglement when the number of particles exceeds the size of two subsystems [63]. In both these cases, the discord and geometric discord between two qubits in a tripartite system goes to 0 as the size of the third subsystem is increased. It is known that the average Q measure for Haar distributed states of N qubits, for large N, goes as $1 - 3/2^N$ [62]. In terms of j $(=N/2)$ it equals $1 - 3/2^{2j}$, implying that the measure tend to 1 for large j. But, the rate at which it approaches 1 is much faster than that for eigenvectors of the COE ensemble corresponding to the kicked top in the globally chaotic case. In contrast to the standard Gaussian or circular ensemble, the random matrix ensemble appropriate for the kicked top is the COE with additional particle exchange symmetry. Hence, this ensemble displays properties different from those of the standard circular or Gaussian ensembles as far as the quantum correlations are concerned.

Interestingly, it is found numerically in the globally chaotic case that $D^G = 0.317D - 0.018$ holds good. This is sshown in Figs. 3, 4, 5, and 9. Such a simple relation relating the Q measure and the discord or geometric discord could not be discerned. It is known that for two-qubit states, the discord and geometric discord are related to each other by $D^G \geqslant D^2/2$ [17,20,64]. This inequality is respected throughout numerical simulations performed here.

VII. SUMMARY AND CONCLUSIONS

In this paper, we have investigated the effect of classical bifurcations on measures of quantum correlations such as the quantum discord, geometric discord, and Meyer and Wallach Q measure using the kicked top as a model of the quantum chaotic system. In a related work [29], the signature of classical chaos in the kicked top was found in the dynamics of quantum discord and this work explores this relation in the more general context of quantum correlations including multipartite entanglement. The suitability of the kicked top is due to the fact that it can be represented as a collection of qubits. Most importantly, this system has been realized in experiments [46]. A prominent feature in its phase space is the period 1 fixed point whose bifurcation is associated with the quantum discord climbing from nearly 0 to a value that is in agreement with the numerically determined random matrix equivalent. The transition in the quantum discord reflects the qualitative change in

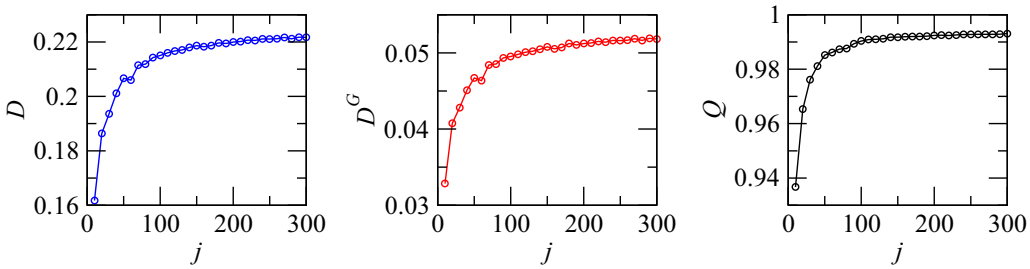

FIG. 9. Variation of time-averaged quantum correlations (circles) as a function of j for the globally chaotic case ($k = 10$).

the classical phase space: from domination by an elliptic island to a largely chaotic sea with a few small elliptic islands. The other measures we have reported here, namely, the geometric discord and Meyer and Wallach Q measure, both display trends similar to those of the quantum discord. Other measures of quantum correlations can be expected to display qualitatively similar results. We have also presented numerical results for the random matrix averages of these quantum correlation measures.

In general, as a function of the chaos parameter, quantum discord can be expected to increase under the influence of a period-doubling bifurcation. However, after the bifurcation has taken place, saturation to the random matrix average will depend on the qualitative nature of dynamics in the larger neighborhood around the fixed point. It must also be pointed out that these results have been obtained through time evolution of a spin-coherent state placed initially on an elliptic island undergoing bifurcation. For reasonably large elliptic islands, equivalent results could have been obtained by considering the Floquet states of the kicked top as well.

We have also investigated the fate of quantum correlations in the semiclassical limit as the Planck volume tends to 0. In the context of the kicked top, this limit translates as $j \to \infty$. In the case of bifurcation associated with larger islands, as in $k \leqslant 2$, the measures of quantum correlations decrease as a function of j and tend to 0 through a slow, approximately power-law decay. In the case of bifurcation associated with smaller islands and the creation of higher order periodic cycles the average decay of quantum correlations is evident but marked by strong fluctuations. The quantum correlation measures reported here have been obtained as that for the time average of an evolving spin-coherent state placed initially at a chosen position in phase space. However, we note that if the spin-coherent state is placed instead in the chaotic sea initially, then a different behavior is obtained. As a function of j, in this case, the quantum correlation measures increase and are saturated to a constant value that can be understood based on eigenvectors of the appropriate random matrix ensemble. Evaluation of the exact analytical expression for the average Q measure for the eigenvectors of the corresponding circular unitary ensemble is carried out and agrees very well that for the eigenvectors of the Floquet operator in the globally chaotic case.

All the results presented in this work emphasize the special role played by the bifurcations and the associated regular phase-space regions in modifying general expectations for the quantum correlations based on random matrix equivalents. These results are important from the experimental point of view, as the kicked top was first implemented in a system of laser-cooled cesium atoms [46]. Recently this model was implemented using superconducting qubits [5]. Here the time-averaged von Neumann entropy has shown a very close resemblance, despite the presence of decoherence, with the corresponding classical phase-space structure for given parameter values [5]. Hence, the detailed effects of bifurcations presented here should be amenable to experiments as well. The scaling of quantum correlations with the total spin should also be observable with fewer than about 10 superconducting qubits.

ACKNOWLEDGMENTS

We are very grateful to acknowledge many discussions with Vaibhav Madhok, T. S. Mahesh, Jayendra Bandyopadhyay, and Arul Lakshminarayan. U.T.B. acknowledges funding from the National Post Doctoral Fellowship (NPDF) of DST-SERB, India, file no. PDF/2015/00050.

APPENDIX: EXACT EVALUATION OF $\langle Q \rangle_E$

In this Appendix an exact evaluation of the ensemble average of the Meyer and Wallach Q measure is calculated. The states in the ensemble have identical qubits and remain unchanged under qubit exchange. As explained in Sec. III one needs to use the symmetric subspace spanned by the basis states $\{|j,m\rangle; (m = -j, -j+1, \ldots, j)\}$. Any pure state $|\phi\rangle$ in this basis is given as

$$|\phi\rangle = \sum_{m=-j}^{j} a_m |j,m\rangle, \quad \text{where} \quad \sum_{m=-j}^{j} |a_m|^2 = 1. \tag{A1}$$

In this case the Q measure is given as

$$Q = 1 - \frac{4}{(2j+1)^2}(\langle S_z\rangle^2 + \langle S_+\rangle\langle S_-\rangle), \tag{A2}$$

where S_z and $S_\pm$ are collective spin operators such that $S_z|j,m\rangle = m|j,m\rangle$ and $S_\pm|j,m\rangle = \sqrt{(j \mp m)(j \pm m + 1)}|j,m \pm 1\rangle$ [58]. The ensemble average is carried out over the states such that they have the statistical properties of the eigenvectors of the COE ensemble. For state $|\phi\rangle$ one obtains the following expression for the expectation:

$$\langle S_z\rangle = \sum_{m=-j}^{j} m|a_m|^2. \tag{A3}$$

This gives

$$\begin{aligned}\langle S_z\rangle^2 &= \sum_{m,n=-j}^{j} mn|a_m|^2|a_n|^2 \\ &= \sum_{m=n} m^2|a_m|^4 + \sum_{m\neq n} mn|a_m|^2|a_n|^2.\end{aligned} \tag{A4}$$

Now, an exact RMT ensemble average is carried out [45,65]. First, one obtains

$$\langle\langle S_z\rangle^2\rangle_E = \sum_{m=n} m^2\langle|a_m|^4\rangle_E + \sum_{m\neq n} mn\langle|a_m|^2|a_n|^2\rangle_E. \tag{A5}$$

It should be noted that the first expectation is for a given state $|\phi\rangle$ and the second expectation with subscript E denotes the ensemble average over all $|\phi\rangle$ having statistical properties of COE eigenvectors. Using the RMT ensemble averages [45,65]

$$\begin{aligned}\langle|a_m|^4\rangle_E &= \frac{3}{(2j+1)(2j+3)}, \\ \langle|a_m|^2|a_n|^2\rangle_E &= \frac{1}{(2j+1)(2j+3)},\end{aligned} \tag{A6}$$

one obtains

$$\langle\langle S_z\rangle^2\rangle_E = \frac{3}{(2j+1)(2j+3)}\sum_{m=n} m^2 + \frac{1}{(2j+1)(2j+3)}\sum_{m\neq n} mn. \quad \text{(A7)}$$

The first summation in the above equation is calculated as follows:

$$\sum_{m=-j}^{j} m^2 = 2\sum_{m=1}^{j} m^2 = \frac{j(j+1)(2j+1)}{3}. \quad \text{(A8)}$$

The second summation is now calculated. Consider the equality,

$$\left(\sum_{m=-j}^{j} m\right)\left(\sum_{m=-j}^{j} n\right) = 0. \quad \text{(A9)}$$

This gives

$$\sum_{m,n} mn = \sum_{m=n} m^2 + \sum_{m\neq n} mn = 0. \quad \text{(A10)}$$

Thus,

$$\sum_{m\neq n} mn = -\sum_{m=n} m^2 = \frac{-j(j+1)(2j+1)}{3}. \quad \text{(A11)}$$

The ensemble average in Eq. (A5) is given as follows:

$$\langle\langle S_z\rangle^2\rangle_E = \frac{2j(j+1)(2j+1)}{3(2j+1)(2j+3)}. \quad \text{(A12)}$$

Considering the average of operators $S_\pm$ for state $|\phi\rangle$,

$$\langle S_\pm\rangle = \sum a_m a^*_{m\pm1}\sqrt{(j\mp m)(j\pm m+1)}. \quad \text{(A13)}$$

This gives

$$\langle S_+\rangle\langle S_-\rangle = \sum_{m,n} a_m a^*_{m+1} a_n a^*_{n-1} \times \sqrt{(j-m)(j+m+1)(j+n)(j-n+1)}. \quad \text{(A14)}$$

It can be seen that the ensemble average will have nonzero contribution only when $m = n-1$. Thus,

$$\langle\langle S_+\rangle\langle S_-\rangle\rangle_E = \sum_{m=-j}^{j-1} \langle |a_m|^2 |a_{m+1}|^2\rangle_E (j-m)(j+m+1). \quad \text{(A15)}$$

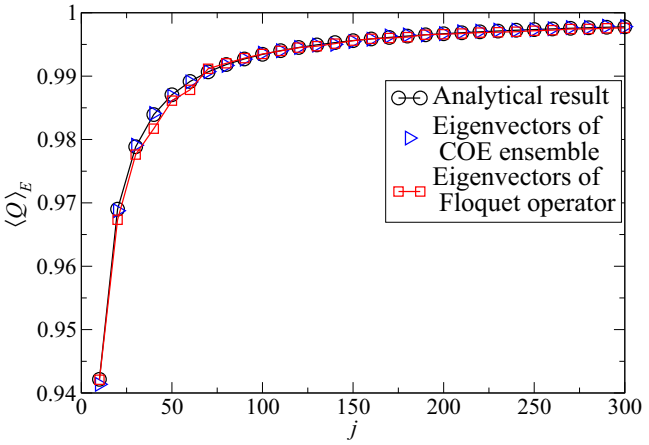

FIG. 10. The average Q measure for the eigenvectors of the COE ensemble and the Floquet operator in the globally chaotic case for the parameter range $10 \leqslant k \leqslant 1000$ and $p = 1.7$ is compared with its analytical expression given in Eq. (14).

Using Eq. (A6) the following is obtained:

$$\langle\langle S_+\rangle\langle S_-\rangle\rangle_E = \frac{1}{(2j+1)(2j+3)}\sum_{m=-j}^{j-1}(j-m)(j+m+1). \quad \text{(A16)}$$

We calculate the summation as follows:

$$\sum_{m=-j}^{j-1}(j-m)(j+m+1) = \sum_{m=-j}^{j-1}(j^2+j-m^2-m) = 2j(j^2+j) - \sum_{m=-j}^{j-1} m - \sum_{m=-j}^{j-1} m^2 = 2j(j^2+j) + j + j^2 - \frac{j(j+1)(2j+1)}{3}. \quad \text{(A17)}$$

Thus,

$$\langle\langle S_+\rangle\langle S_-\rangle\rangle_E = \frac{2j(j+1)}{3(2j+3)}. \quad \text{(A18)}$$

Using Eqs. (A12) and (A18) the final expression for the ensemble average of the Q measure, denoted $\langle Q\rangle_E$, is given as follows:

$$\langle Q\rangle_E = 1 - \frac{16j(j+1)}{3(2j+3)(2j+1)^2}. \quad \text{(A19)}$$

This analytical expression is plotted in Fig. 10.

[1] H.-J. Stöckmann, *Quantum Chaos: An Introduction* (Cambridge University Press, Cambridge, UK, 1999).

[2] A. D. Stone, Phys. Today **58**, 37 (2005).

[3] M. C. Gutzwiller, *Chaos in Classical and Quantum Mechanics* (Springer-Verlag, New York, 1990).

[4] M. L. Mehta, *Random Matrices*, 3rd ed. (Elsevier Academic Press, London, 2004).

[5] C. Neill, P. Roushan, M. Fang, Y. Chen, M. Kolodrubetz, Z. Chen, A. Megrant, R. Barends, B. Campbell, B. Chiaro *et al.*, Nat. Phys. **12**, 1037 (2016).

[6] A. Lakshminarayan, Phys. Rev. E **64**, 036207 (2001).

[7] M. S. Santhanam, V. B. Sheorey, and A. Lakshminarayan, Phys. Rev. E **77**, 026213 (2008).

[8] C. H. Bennett, D. P. DiVincenzo, C. A. Fuchs, T. Mor, E. Rains, P. W. Shor, J. A. Smolin, and W. K. Wootters, Phys. Rev. A **59**, 1070 (1999).
[9] J. Niset and N. J. Cerf, Phys. Rev. A **74**, 052103 (2006).
[10] M. Horodecki, P. Horodecki, R. Horodecki, J. Oppenheim, A. Sen, U. Sen, and B. Synak-Radtke, Phys. Rev. A **71**, 062307 (2005).
[11] E. Knill and R. Laflamme, Phys. Rev. Lett. **81**, 5672 (1998).
[12] A. Datta, A. Shaji, and C. M. Caves, Phys. Rev. Lett. **100**, 050502 (2008).
[13] G. Passante, O. Moussa, D. A. Trottier, and R. Laflamme, Phys. Rev. A **84**, 044302 (2011).
[14] H. Ollivier and W. H. Zurek, Phys. Rev. Lett. **88**, 017901 (2001).
[15] L. Henderson and V. Vedral, J. Phys. A: Math. Gen. **34**, 6899 (2001).
[16] B. Dakić, V. Vedral, and Č. Brukner, Phys. Rev. Lett. **105**, 190502 (2010).
[17] S. Luo and S. Fu, Phys. Rev. A **82**, 034302 (2010).
[18] A. J. Leggett and A. Garg, Phys. Rev. Lett. **54**, 857 (1985).
[19] S. Virmani and M. B. Plenio, Phys. Lett. A **268**, 31 (2000).
[20] K. Modi, A. Brodutch, H. Cable, T. Paterek, and V. Vedral, Rev. Mod. Phys. **84**, 1655 (2012).
[21] S. Luo, Phys. Rev. A **77**, 042303 (2008).
[22] M. Ali, A. R. P. Rau, and G. Alber, Phys. Rev. A **81**, 042105 (2010).
[23] J. Maziero, L. C. Céleri, R. M. Serra, and V. Vedral, Phys. Rev. A **80**, 044102 (2009).
[24] T. Werlang, S. Souza, F. F. Fanchini, and C. J. Villas Boas, Phys. Rev. A **80**, 024103 (2009).
[25] L. C. Céleri, J. Maziero, and R. M. Serra, Int. J. Quantum Info. **09**, 1837 (2011).
[26] A. Maldonado-Trapp, P. Solano, A. Hu, and C. W. Clark, arXiv:1604.07351.
[27] H. Singh, T. Chakraborty, P. K. Panigrahi, and C. Mitra, Quant. Info. Proc. **14**, 951 (2015).
[28] E. Moreva, M. Gramegna, M. A. Yurischev, and M. Genovese, arXiv:1605.01206v1.
[29] V. Madhok, V. Gupta, D.-A. Trottier, and S. Ghose, Phys. Rev. E **91**, 032906 (2015).
[30] T. Kapitaniak, *Chaos for Engineers: Theory, Applications, and Control* (Springer-Verlag, Berlin, 2000).
[31] D. A. Meyer and N. R. Wallach, J. Math. Phys. **43**, 4273 (2002).
[32] A. Datta, Ph.D. thesis, The University of New Mexico, 2008.
[33] W. H. Zurek, Ann. Phys. (Berlin) **9**, 855 (2000).
[34] V. Madhok and A. Datta, Phys. Rev. A **83**, 032323 (2011).
[35] Z. Huang and D. Qiu, Quant. Info. Proc. **15**, 1979 (2016).
[36] A. S. M. Hassan, B. Lari, and P. S. Joag, Phys. Rev. A **85**, 024302 (2012).
[37] S. Rana and P. Parashar, Phys. Rev. A **85**, 024102 (2012).
[38] D. Girolami and G. Adesso, Phys. Rev. Lett. **108**, 150403 (2012).
[39] A. Lakshminarayan and V. Subrahmanyam, Phys. Rev. A **71**, 062334 (2005).
[40] J. Karthik, A. Sharma, and A. Lakshminarayan, Phys. Rev. A **75**, 022304 (2007).
[41] W. G. Brown, L. F. Santos, D. J. Starling, and L. Viola, Phys. Rev. E **77**, 021106 (2008).
[42] N. Lambert, C. Emary, and T. Brandes, Phys. Rev. A **71**, 053804 (2005).
[43] G. K. Brennen, Quantum Info. Comput. **3**, 619 (2003).
[44] A. J. Scott, Phys. Rev. A **69**, 052330 (2004).
[45] F. Haake, *Quantum Signatures of Chaos*, 3rd ed. (Springer, Berlin, 2010).
[46] S. Chaudhury, A. Smith, B. E. Anderson, S. Ghose, and P. S. Jessen, Nature **461**, 768 (2009).
[47] M. Lombardi and A. Matzkin, Phys. Rev. E **83**, 016207 (2011).
[48] S. Ghose, R. Stock, P. Jessen, R. Lal, and A. Silberfarb, Phys. Rev. A **78**, 042318 (2008).
[49] P. A. Miller and S. Sarkar, Phys. Rev. E **60**, 1542 (1999).
[50] J. N. Bandyopadhyay and A. Lakshminarayan, Phys. Rev. Lett. **89**, 060402 (2002).
[51] J. N. Bandyopadhyay and A. Lakshminarayan, Phys. Rev. E **69**, 016201 (2004).
[52] G. Stamatiou and D. P. K. Ghikas, Phys. Lett. A **368**, 206 (2007).
[53] F. Haake, M. Kus, and R. Scharf, Z. Phys. B **65**, 381 (1987).
[54] F. T. Arecchi, E. Courtens, R. Gilmore, and H. Thomas, Phys. Rev. A **6**, 2211 (1972).
[55] R. J. Glauber and F. Haake, Phys. Rev. A **13**, 357 (1976).
[56] R. R. Puri, *Mathematical Methods of Quantum Optics* (Springer, Berlin, 2001).
[57] X. Wang and K. Mølmer, Eur. Phys. J. D **18**, 385 (2002).
[58] H. Ming-Liang and X. Xiao-Qiang, Chinese Phys. B **17**, 3559 (2008).
[59] A. Peres and D. Terno, Phys. Rev. E **53**, 284 (1996).
[60] M. Kus, J. Mostowski, and F. Haake, J. Phys. A: Math. Gen. **21**, L1073 (1988).
[61] U. T. Bhosale, S. Tomsovic, and A. Lakshminarayan, Phys. Rev. A **85**, 062331 (2012).
[62] A. J. Scott and C. M. Caves, J. Phys. A: Math. Gen. **36**, 9553 (2003).
[63] V. S. Vijayaraghavan, U. T. Bhosale, and A. Lakshminarayan, Phys. Rev. A **84**, 032306 (2011).
[64] D. Girolami and G. Adesso, Phys. Rev. A **83**, 052108 (2011).
[65] N. Ullah and C. E. Porter, Phys. Lett. **6**, 301 (1963).